

***In-situ* XAFS study of Fe epitaxially grown by MBE on GaAs(001)-4x6**

R.A. Gordon, E.D. Crozier*, D.-T. Jiang¹, P.S. Budnik, T.L. Monchesky² and B. Heinrich
Department of Physics, Simon Fraser University, Burnaby, BC, Canada V5A 1S6

¹present address: Canadian Light Source, Saskatoon, SK, Canada S7N 5C6

²present address: Department of Physics, Dalhousie University, Halifax, NS, Canada B3H 3J5

*corresponding author: phone (604) 291-4827, fax (604) 291-3592, e-mail crozier@sfu.ca

To be submitted to Surface Science

Abstract

Using the molecular beam epitaxy facilities of the Pacific Northwest Consortium Collaborative Access Team at the Advanced Photon Source, we have prepared and examined *in-situ* the structures of iron films deposited on the 4x6-reconstructed surface of GaAs(001) with thicknesses ranging from 0.5 to 30 monolayers. We have employed the polarization-dependent X-ray Absorption Fine Structure (XAFS) technique in total reflection mode to examine the iron environment and compare in-plane to out-of-plane structure in these films. The X-ray Absorption Near Edge Structure (XANES) does not indicate a change in the energy position of the iron K-absorption edge with thickness, but there are features that shift to lower energy just above the edge, and become less evident, with decreasing thickness owing to changes in bonding and increasing influence of substrate atoms on the iron. Near 4 monolayers, a transition from island to layer-by-layer growth modes is accompanied by the observation of a distortion of the iron to a body-centered tetragonal structure (as compared to bulk body-centered cubic iron) with a c/a ratio of 1.030(8), with no thickness dependence observed to 30 monolayers.

Keywords: molecular beam epitaxy, XAFS, growth, surface structure, iron, gallium arsenide, magnetic films

1. Introduction

Magnetic nanostructures based on the system of iron films on the (001) surface of gallium arsenide continue to attract considerable experimental and theoretical interest [1-6]. Ongoing concerns in this system involve the origins of uniaxial magnetic anisotropy and the potential for the films to react with the substrate to produce a magnetic “dead” layer [5-10]. The Ga-rich 4x6 surface [11] has been shown to yield high-quality epitaxial iron films with no magnetic dead layer, but with some migration of As atoms from the substrate to the surface of the iron [8]. In this work, we focus on films prepared on the 4x6 reconstructed surface.

The growth mechanism for iron films on the 4x6 surface of GaAs(001) proceeds through island formation (Volmer-Weber) to layer-by-layer (quasi-Frank-van-der-Mewe), with the transition between modes occurring near 4 monolayer (ML) deposition [8]. A high density of macroscopic defects has been observed for a 20 nm thick film [12]. Studies have been done on the evolution of the magnetic behavior, morphology and stress of these films [9,12,13], but the body of knowledge, though extensive, still lacks an understanding of the film structure as it relates to the transition in growth modes and the development of the reported body-centered tetragonal (bct) distortion (from body-centered cubic (bcc)) in films near 10 ML thickness [14]. Using the *in-situ* molecular beam epitaxy (MBE) capabilities at the Pacific Northwest Consortium (PNC-CAT) beamline [15], we have performed *in-situ* polarization-dependent X-ray Absorption Fine Structure (XAFS) studies of iron on GaAs(001)-4x6 for thicknesses from 0.5 to 30 ML.

Polarization-dependent XAFS functions by orienting the electric field of a linearly-polarized X-ray beam along (nearly along, grazing) the desired orientation of a single-crystalline material, such as an epitaxial thin film [16-20]. The absorption of the linearly polarized X-rays

causes the ejected photoelectrons to have a dipole-like distribution - high probability of the photoelectron being emitted along the direction of polarization and negligible probability perpendicular to the polarization. How this influences backscattering from nearby atoms, which affects the XAFS oscillations in the absorption spectrum, is illustrated for a body-centered-cubic-related structure in Figure 1. An absorbing atom, **0**, has 8 nearest neighbours, **1** and 6 second-nearest neighbours, **2** (Fig. 1a.). For X-rays incident along the $\langle 001 \rangle$ direction (perpendicular to the substrate), atoms **1** in the first shell all contribute, but only the atoms **2** at $\pm c$ -lattice constant contribute to the second shell (Fig. 1b.). For polarization along $\langle 110 \rangle$ (Fig. 1c.), only half the atoms labeled **1** contribute to the first shell and the 4 atoms labeled **2** in the *ab*-plane contribute to the second shell. We have applied this method to the iron films being studied in order to extract details on the nearest-neighbours and the second nearest-neighbours, information which contains the lattice constants and permits an examination of the distortion from body-centered cubic.

2. Experimental

Samples were prepared using the MBE endstation (MBE1) on the undulator beamline of the PNC-CAT at the Advanced Photon Source. The MBE1 system has a base pressure of 2×10^{-10} Torr. Samples were mounted on a custom positioner (Thermionics Northwest GB-16 based) that allows wafers to be oriented anywhere from normal incidence to grazing angle for polarization-dependent XAFS measurements. Epiready α -type GaAs substrates (American Xtal Technology) were introduced to the vacuum system, given a 1 hour thermal desorption treatment at 600°C , then, when cooled to room temperature, sputtered with 500eV Ar^+ for 3 hours at an Argon pressure of 2×10^{-5} Torr. Substrates were then annealed and monitored by Reflection High Energy

Electron Diffraction (RHEED) until the 4x6 reconstruction was achieved [8]. Substrates were permitted to cool to room temperature before deposition of the iron films. Films of nominal thicknesses 0.5, 2, 3.5, 5, 6, 9.3, 15, 16, and 30 ML were deposited using Omicron EFM3 evaporators at rates between 0.5 and 1M L/minute and, again, monitored by RHEED, with either the oscillations of the intensity of the specular spot, or the flux as measured by the evaporator being used to estimate thickness. The 2 ML, 15 ML and 30 ML samples were prepared on top of the 0.5 ML, 3.5 ML and 16 ML samples, respectively. For these second depositions, no RHEED oscillations were observed.

XAFS measurements were made with the X-ray polarization vector in and out of the plane of the substrate. To minimize distortion of the spectra due to anomalous dispersion effects in the sample and adjacent substrate [16], the angle of incidence was set to approximately 2/3 of the critical angle ($\theta_c \sim 0.4^\circ$) for total reflection at 250 eV above the Fe K-edge. In addition, for the 16 and 30 ML samples, aluminum foil filters were inserted at the entrance to the fluorescence chamber to attenuate the enhanced fluorescence caused by interference of the evanescent waves in the sample-substrate structure. For out-of-plane measurements, the polarization was within 0.25° of the $\langle 001 \rangle$ direction. For in-plane measurements, the polarization was oriented within 2° of the $\langle 110 \rangle$ direction (i.e. parallel to the x4 reconstruction direction) for all but the 9.3ML sample, where the $\langle 010 \rangle$ direction was used. Small azimuthal adjustments were made within a 2° margin to shift small Bragg peaks contaminating the fluorescence signal so the peaks could be removed in processing. The silicon (111) double crystal monochromator on the PNC-CAT insertion device line [15] was detuned by 25% at 7500eV to reduce harmonic energies in the X-ray beam. Data were collected in both fluorescence and total-electron-yield modes though only fluorescence is considered in this work. For 3.5 ML and thicker samples, an argon-filled

fluorescence ion chamber was used [21]. For the 2 ML and 0.5 ML samples, a solid state Ge(Li) detector was used. All fluorescence intensities, I_f , were normalized to the incident x-ray intensity, I_0 , measured with a He-filled, two-parallel-plate-electrode ionization chamber. Typically, 4 scans of ion chamber data were averaged for subsequent analysis, while 10 scans of solid state detector data were used. A reference iron foil was also measured in transmission using He-filled ionization chambers.

3. Results and Discussion

X-ray Absorption Near Edge Structure (XANES) spectra for select thicknesses of iron are given in Fig. 2 along with their first derivatives. XANES at the Fe $L_{2,3}$ edges of iron films on sputtered (but not annealed/reconstructed) GaAs(001) have indicated an increase in the number of d-holes on the Fe [22] - up to 1 full hole near 5 ML thickness- and was attributed to charge transfer to the substrate. The XANES at the Fe K-edge shown in Fig. 2 indicate features near 7120eV and 7128 eV, evidenced by peaks in the derivatives, that shift to lower energy with decreasing thickness, but the edge-position itself at 7111eV remains unchanged for both polarizations. This is better illustrated in Fig. 3, where the 5 ML in-plane and out-of-plane XANES spectra are directly compared to iron foil and iron (II) oxide. The loss of 2 electrons on going from iron metal to iron oxide has a very pronounced effect on the near edge region through a combination of structural and electronic changes. The differences between the films and iron metal are more subtle. The features at 7120 and 7128, which can be associated with transitions between 1s core and unoccupied 4p states, also become less-pronounced with decreasing thickness. That this is attributable to increasing influence of the substrate is without question, but the nature of the interaction remains to be answered. The relative amounts of Fe, Ga and As in

the interfacial/surface region are changing. It will be shown later in the Extended XAFS (EXAFS) analysis, however, that there is no change in the structural distortion to bct for films 5 ML or thicker. With no apparent iron K-edge-shift, there cannot be any dramatic change in screening of the K-shell. With the 1s-4p features shifting to lower energy, this may be an indication that some Fe 4p states (or hybridized 3d4sp) that would normally be unoccupied in bulk Fe are being used in bonding (largely covalent in nature) with Ga and As 4p states. The increase in d-holes observed at the $L_{2,3}$ edges could then be attributed to charge transfer from 3d to 4s,p states on the iron that have shifted below the Fermi level, resulting in a negligible change in core screening on the iron.

EXAFS interference functions, $\chi(k)$, were extracted from the normalized fluorescence data using the program, AUTOBK [23]. The zero of the k-space scale was taken to be at the energy of the first inflection point in the mass absorption coefficient $\mu(E)$ which is proportional to the ratio I_f/I_0 . Figure 4 shows the $\chi(k)$ for both out-of-plane (fig. 4a.) and in-plane (fig. 4b.) measurements as well as the reference iron foil. For the thinnest two samples, both polarizations reveal little beyond what appears to be a single frequency in $\chi(k)$. As the thickness increases, additional structure appears that corresponds to the growth of the higher shells evident in the Fourier transforms in Figure 5. Differences exist between the in-plane and out-of-plane that persist up to and including the 30ML data. This contrast is most apparent in the interference functions in the range 2.3 - 7 \AA^{-1} . The in-plane data for thicker samples strongly resemble the reference foil. The out-of-plane data strongly differs from the foil and in-plane $\chi(k)$'s in two main regions: in the reduced feature near 4.6 \AA^{-1} and in the absence of a feature near 6 \AA^{-1} . This is a strong indication that a structural distortion is present up to the 30 ML sample, the highest thickness measured.

The Fourier transforms in fig. 5 were taken with a k^2 weighting and 10% Gaussian window over a k -space range typically $2.4 - 14 \text{ \AA}^{-1}$. Overall, the resemblance to bcc iron is quite strong in that there are three main peaks of note in the transform. For bcc iron (fig. 1a), the first peak, near 2.2 \AA contains both the nearest neighbour (n.n., corner atoms **1** in fig 1a) and next-nearest neighbour (lattice constant away, atom **2**). The second (middle) peak is dominated by backscattering along the face diagonal (most simply visualized by considering an atom **1** in fig 1a to be the absorber and the scatterer another atom **1** along the face diagonal of the unit cell), but also contains some multiple (three-leg) scattering that tails into the first peak. These are triangular paths, identified when considering FEFF7 [24] calculations, that involve the emitted photoelectron either: a) traveling from the absorbing atom (labeled **0** in fig. 1) to an atom at the corner of the unit cell (atom **1**) to another corner atom **1** along a cell edge before returning to the absorber, **0**; or b) traveling from **0** to **1** to an atom **2** nearby before returning to **0**. The third peak, near 4.5 \AA is dominated by backscattering and focused multiple scattering along the body diagonal of the unit cell. Vestiges of this peak remain even down to 3.5 ML, even though few unit cells are present for the out-of-plane polarization. This could be due to the multiple-scattering paths that only involve the nearest neighbours - of the sort $\{\mathbf{0} \text{ to } \mathbf{1} \text{ to } \mathbf{1}_{\text{opposite corner}} \text{ to } \mathbf{0}\}$ or $\{\mathbf{0} \text{ to } \mathbf{1} \text{ to } \mathbf{0} \text{ to } \mathbf{1} \text{ to } \mathbf{0}\}$ which would persist even if most of the atoms do not have a neighbour located a body-diagonal distance away.

The polarization-dependent data were fit in R-space using FEFF7 simulations in the program WINXAS [25]. For consistency from thickest to thinnest sample, only the first peak (n.n., lattice constant and associated multiple-scattering paths) in the transforms were used. Model EXAFS interference functions were constructed using FEFF7 and a modified version of the EXAFS equation:

$$\chi_{model}(k) = \sum_j \frac{S_o^2 N_j F_j(k)}{kR_j^2} e^{(-2k^2\sigma_j^2)} e^{(-\frac{2R_j}{\lambda})} \sin(2kR_j + \delta_j(k)) \quad (1)$$

used in WINXAS. In equation 1, with k being the magnitude of the photoelectron wave vector, the effective number of atoms N are located at distance R with mean-square-relative-displacement σ^2 and possess effective scattering amplitudes $F(k)$, while the photoelectron has mean-free-path, $\lambda(k)$ and phase shift $\delta(k)$ on traveling through the differing atomic potentials; and the sum is done over all scattering paths, j . FEFF7 calculations (in the curved-wave approximation) provide the $\lambda(k)$, $\delta(k)$ and $F(k)$ for each atom and scattering path at a given distance in the model structure that are used in refining distances and other parameters in the fit structure. The polarization dependence of the photoelectron scattering is also included by FEFF7 in $F(k)$. S_o^2 is a slowly varying function of k describing reduction of the scattered amplitude due to multiple scattering effects. In our analysis we have treated it as an adjustable scaling parameter.

From out-of-plane measurements, the c -axis distance is extracted, while from in-plane, the average a -axis value is obtained. In constructing a structural model to fit the Fe K-edge EXAFS data it is necessary to include contributions from both Ga and As in the substrate. Since it is known that up to one monolayer of As diffuses from the substrate and segregates to the free Fe surface [8], the model must also include an overlayer of As. In first principle calculations of Fe on GaAs(001) it has been shown if kinetically possible, Fe will substitute for Ga independent of Ga-Ga or As-As terminations at the surface [1]. In fitting Fe K-edge EXAFS data, there is insufficient difference in their scattering amplitudes and phase shifts to distinguish Ga from As. Indeed it is a challenge, in small to moderate concentration, to distinguish either species from Fe.

To simplify the structural model, the amplitude and phase shifts of Ge were used to represent Ga and As.

The data were fit to an idealized model of a thin Fe film with infinite smooth sheets capped above and below by Ge representing the As overlayers and Ga rich substrate surface, with a reduction in average coordination numbers appropriate to the film thickness [26]. Theoretical XAFS amplitudes and phases were calculated in FEFF7 as alloys of varying composition (0 %, 12.5 %, 25 % & 50 % based on the number of non-Fe atoms in the first nearest-neighbour shell). This, with the exception of the Ge approximation, is similar to the theoretical treatment of Mirbt et al [1], where Ga-diffusion and As-capping were considered. With increasing film thickness, the influence of the substrate atoms decreases. For 9.3 ML and thicker, the influence of the Ga and As atoms became insignificant - fitting with a pure-Fe model gave comparable results. Deviations from the ideal model with infinite smooth sheets are likely to manifest in the form of finite sheets and surface roughness. If less than 1 ML of arsenic migrates to the surface, then the capped model overestimates the concentration of As atoms in the EXAFS shells. The physical manifestation of all three of these deviations from the model would be reductions in co-ordination. Since co-ordination numbers are fixed according to the model and the film thickness, S_0^2 acting as a scaling parameter compensates and would be reduced instead of N if the film size, roughness or arsenic overlayer are not as assumed in the model.

Fit results are summarized in figure 6. Parameters allowed to vary during the fits were: S_0^2 ; distances, R_i ; mean-square relative displacements (msrd) σ_i^2 ; and E_0 shift to compensate for differences between the Fermi level calculated in the model and the zero of the k-space scale. The distances and msrds were constrained to be the same for both the iron and impurity atoms.

No difficulties were encountered in fitting that would have mandated a splitting of these two parameters into separate, independent values. Co-ordination numbers N_j were fixed according to the capped-film model for all but the thinnest film, and varied with the nominal film thickness. The S_o^2 values remained in the range of 0.6 to 0.7 for the films 5 ML and thicker, reduced relative to 0.75(2) obtained for the foil, but still indicating large film areas consistent with layer growth. For the 3.5 ML and 2 ML samples, S_o^2 decreased to 0.51(2) and 0.48(2), respectively, which can be attributed to finite island size effects on co-ordination¹.

For the 2 ML and 0.5 ML films, no second nearest neighbour could be extracted from the data. This resulted in a strong dependency on model and on relative amounts of Fe and Ge: the Ge level is comparable to iron at 2 ML, and exceeds the Fe content at 0.5 ML. For 2 ML, a reasonable fit could still be obtained with the capped film model albeit with average n.n. coordination number reduced to 2/3 the bulk value, based on the reduction in S_o^2 . For 0.5 ML, S_o^2 was fixed at 0.65 (transferred from the thicker films) and the relative amounts of Fe and substrate atoms allowed to vary. Doing so for the out-of-plane orientation favored the substrate atoms roughly 6:1.5 over the Fe, with summed co-ordination of ~ 7.5 atoms in the first shell.

¹ This reduction can be used to give a rough estimate of our island size. First-shell coordination numbers scale as $((\text{thickness} - 1)/\text{thickness in monolayers})$ for an (uncapped) infinite sheet. A similar scaling behavior can be applied for the in-plane dimensions. Since S_o^2 and N_1 are directly correlated, by considering the square root of the ratio of the S_o^2 values for thin (0.5) and thicker films (0.65 on average), and already considering finite out-of-plane thickness when fitting, we obtain a rough estimate of 8 ML for island side, or approximately 120\AA^2 island area. This is a lower limit that assumes square islands and does not consider anisotropy in island shape, nor roughness.

Fitting with no Fe in the shell gave similar results for R_1 and σ_1^2 , but with $N_1 \sim 8$. The in-plane 0.5 ML data could not be fit with only substrate atoms in the shell. Allowing the amounts of Fe and substrate atoms to vary resulted in only Fe, with $N_1 \sim 2.3$ atoms. While the absence of substrate atoms in this shell is puzzling, we do have two possible clues as to why this may be so: 1) the reconstructed surface [11] possesses channels that would permit linear arrangements of iron atoms at low coverage along the $\langle 110 \rangle$ and $\langle -110 \rangle$ directions; and 2) the slice projections along $\langle 1-10 \rangle$ calculated by Mirbt et al [1] indicate iron as the nearest in-plane neighbour with the nearest substrate atom neighbours being 2 atoms oriented orthogonal to the iron neighbour (and hence would have a negligible contribution to an in-plane-polarized XAFS measurement). However, this does not resolve why we observe ~ 8 nearest neighbours for the out-of-plane results.

For 5 ML and thicker samples, in both polarizations, both first and second nearest neighbour distances show little variation. The R values plotted in fig. 6 have had offset corrections of $\sim 0.01 \text{ \AA}$ applied, based on fits to the iron foil standard. The n.n. distances obtained from out-of-plane measurements for 5 ML and higher, $\langle R_{\text{out}} \rangle = 2.481(4) \text{ \AA}$, are comparable to that for bcc iron (2.4824 \AA). The in-plane n.n. results for films measured along $\langle 110 \rangle$ (i.e. not the 9.3 ML data which was measured along $\langle 010 \rangle$) are consistently lower than the out-of-plane results by 0.008 \AA on average ($\langle R_{\text{in}} \rangle = 2.473(4) \text{ \AA}$ - within error individually, but noticeably lower for the average). Both the c -axis and average a -axis deviate from bcc Fe, as noted for films near 10 ML [14], and are indicative of the distortion to a body-centered tetragonal structure (or pseudo-tetragonal for measurements along $\langle 110 \rangle$ since only an average in-plane lattice constant is determined). In considering films from 5 ML to 30 ML, we find the average out-of-plane lattice constant, c_{film} , to be $2.915(17) \text{ \AA}$, and the average in-plane value, a_{film} , to be

2.830(14) Å. The in-plane value is in good agreement with lattice-matching to the GaAs substrate ($a/2 = 2.827$ Å). This results in a mean value for the c/a ratio of 1.030(8) with a Δc ($c_{film} - c_{foil}$) of 0.049(17) Å and Δa ($a_{film} - a_{foil}$) of -0.037(14) Å. Macroscopic elasticity theory [14, 27-31] relates the in-plane and out-of-plane stresses: $\Delta c/\Delta a = -2c_{12}/c_{11}$, and, using the known elastic constants c_{ij} for iron [30,31], this ratio should be -1.212. The average results for the films gives -1.3(7), in good agreement, even with the large error. The absence of a thickness dependence to the distortion for films thicker than 4 ML also allays previous concerns [14] regarding perpendicular magnetic anisotropy measurements [8], where a thickness dependence to the strain would have necessitated a reinterpretation of the results.

The first principles calculation of Mirbt et al [1] for 5 ML with a 1 ML arsenic cap yielded a theoretical c/a ratio of 1.03 in agreement with our experimental result. In addition they predicted a distortion in-plane to give a contraction along $\langle 110 \rangle$ of 1.83 % and an expansion along $\langle -110 \rangle$ of 0.51 %. This predicted in-plane distortion would cause a splitting of the 8 nearest-neighbour distances (Fig. 1a) into 4 atoms at 2.445 Å (i.e. the atoms indicated in Fig 1c) and 4 at 2.483 Å, with an average of 2.464 Å for the 8 atoms. In our work, with the X-ray polarization perpendicular to the plane of the substrate, we have contributions from all 8 atoms (Fig. 1b) and extract the average distance. With the polarization in the plane along $\langle 110 \rangle$, we examine the 4 nearest-neighbour atoms that are predicted to be contracted. A contraction along $\langle 110 \rangle$ is observed in our work for our 5ML sample: $R_{in-p.} = 2.467(9)$ Å and $R_{out-o.-p.} = 2.482(8)$ Å, with $R_{out-o.-p.}$ representing still the average over all 8 nearest neighbours. The spatial resolution of EXAFS [32] is limited by the finite range of data by the relation $\Delta k \Delta R = \pi/2$. With a k -space range, $\Delta k \lesssim 12$ Å⁻¹, the minimum resolvable separation of two bond lengths is 0.13 Å. Both in-plane and out-of-plane experimental values are approximately 0.02 Å larger than their

corresponding theoretical values, but do follow the theoretical trend. This may be an artifact of fitting since the differences for the 6 ML sample are less noticeable. Additional XAFS measurements with the X-ray polarization vector in the surface along $\langle -110 \rangle$ are necessary to confirm the in-plane distortion in this system at low coverage, complimenting work done on thicker films prepared on the As-rich 2×4 GaAs surface [5] in exploring uniaxial magnetic anisotropy in the Fe/GaAs system.

For thicknesses below 5 ML, in the regime of island growth, a decrease in nearest-neighbour distance is observed for out-of-plane measurements, almost linearly with decreasing thickness. At 0.5 ML, the distance approaches that for the Ga-As bondlength in the substrate (2.448 \AA). If the Fe were occupying tetrahedral vacancies in the upper surface of the GaAs substrate, one could expect this distance, but with coordination number of 4, not 7.5 to 8 as noted in fitting the out-of-plane data. The in-plane result suggests only Fe atoms present as nearest neighbours in-plane, but with a larger distance, at $2.475(9) \text{ \AA}$, than out-of-plane. The Fe cannot, therefore, be merely substituting into the lattice, nor nucleating a bcc-like phase. These results indicate a reaction with the Ga-rich surface to form a separate phase at the surface.

A separate phase forming at the surface has been suggested by the first principles calculations of Mirbt et al [1]. In their work, for a 1 monolayer film, the nearest-neighbour interactions for an out-of-plane polarization would contain only contributions from the substrate, with the Fe-As and Fe-Ga distances calculated to be 2.32 \AA and 2.51 \AA , respectively. Our measured value of the average, at $2.454(8) \text{ \AA}$, is about 0.04 \AA larger than calculation suggests (perhaps due to the use of the Ga-rich 4×6 reconstructed surface), but is comparable. The nearest-neighbour in-plane, based on Figure 6 of reference 1, is exclusively iron and estimated to be approximately 10% further away than the Fe-Ga distance (i.e. about 2.75 \AA) which is

considerably larger than what is observed for the 0.5 ML sample in this work. The polarization dependence (substrate atoms out-of-plane, iron in-plane), however, is consistent. This may not reflect the true nature of the interface for a thicker film since the cessation of growth at such a low coverage, potentially before stable islands have formed, may lead to increased surface reaction.

The mean-square-relative-displacements increase with decreasing thickness, consistent with an increasing ratio of surface to interior atoms (fewer atoms bound inside the film) and may also reflect the increasing influence of substrate atoms within the iron film. Values for the second shell atoms in the out-of-plane polarization plotted in fig. 6 are considerably larger than the nearest-neighbour, in-plane or foil values. This may be due to increased disorder or (surface) roughness in the out-of-plane direction. It may also be due to the strained nature of the film itself. For both polarizations, the nearest-neighbour interactions are largely in-plane, since the nearest-neighbour in a bcc or bct structure is located approximately 36° above the plane (the angle between the $\langle 111 \rangle$ and $\langle 110 \rangle$ directions). Next-nearest neighbour interactions for in-plane are also (entirely) in-plane, but, for the out-of-plane measurements, the next-nearest neighbour is 90° above the plane – entirely out of plane. The out-of-plane direction is the direction of response to the in-plane stress. It is not unreasonable to expect a larger dynamic contribution to the mean-square-relative-displacement in this case, but a temperature-dependent study would be required to confirm this.

4. Conclusions

We have made *in-situ* XAFS measurements on iron films deposited on 4x6-reconstructed

GaAs(001) substrates. Our polarization-dependent study on films from 0.5 to 30 monolayers thick has indicated that, upon achieving layer-by-layer growth above 4 ML, the films possess a structure distorted from the body-centered cubic structure of bulk iron to match the GaAs substrate in-plane, as measured by the average in-plane lattice constant, and expanded out-of-plane with a ratio of lattice axes, $c/a = 1.030(8)$. In-plane results suggest a further distortion from a body-centered tetragonal film structure, but further study is needed. Mean-square-relative-displacements of the average atom in the films are roughly twice as large for the out-of-plane second-nearest-neighbors (lattice constant c away) than for the corresponding in-plane neighbors, consistent with being the direction of relaxation from the in-plane compressive stress.

Below 4 ML, nearest-neighbor distances contract. From measurements with X-ray polarization perpendicular to the substrate, this contraction appears linear, decreasing from 2.48Å (comparable to bulk iron) to 2.45Å (approaching bulk GaAs) with decreasing thickness. Co-ordination results for 0.5 ML, however, do not support substitution of Fe into GaAs but suggest instead some reaction to form a surface phase.

Acknowledgments

This work was supported by operating grants from the Natural Sciences and Engineering Research Council of Canada. PNC-CAT facilities at the Advanced Photon Source, and research at these facilities, are supported by the US DOE Office of Science Grant No. DEFG03-97ER45628, the University of Washington, a major facilities access grant from NSERC, Simon Fraser University and the Advanced Photon Source. Use of the Advanced Photon Source is also supported by the U. S. Department of Energy, Office of Science, Office of Basic Energy Sciences, under Contract No. W-31-109-Eng-38.

References

- [1] S. Mirbt, B. Sanyal, C. Isheden and B. Johansson, *Phys. Rev. B* 67 (2003) 155421.
- [2] T.A. Moore, G. Wastlbauer and J.A.C. Bland, *J. Phys: Condens. Matter* 15 (2003) L407.
- [3] A.A. Veselov, A.G. Veselov, S.L. Vysotsky, A.S. Dzhumaliev and Yu.A. Filimonov, *Zh. Tekh. Fiz.* 72(8) (2002) 139.
- [4] R. Sato and K. Mizushima, *J. Magn. Soc. Jpn.* 27(3) (2003) 106.
- [5] O. Thomas, Q. Shen, P. Schieffer, N. Tournerie and B. Lépine, *Phys. Rev. Lett.* 90 (2003) 017205.
- [6] M. Zölfl, S. Kreuzer, D. Weiss and G. Bayreuther, *J. Appl. Phys.* 87 (2000) 7016.
- [7] M. Doi, B. Roldan Cuenya, W. Keune, T. Schmitte, A. Nefedov, H. Zabel, D. Spoddig, R. Meckenstock and J. Pelzl, *J. Magn. Mater.* 240 (2002) 407.
- [8] T.L. Monchesky, B. Heinrich, R. Urban, K. Myrtle, M. Klaua and J. Kirschner, *Phys. Rev. B* 60 (1999) 10242.
- [9] Y.B. Xu, E.T.M. Kernohan, D.J. Freeland, A. Ercole, M. Tselepi and J.A.C. Bland, *Phys. Rev. B* 58 (1998) 890.
- [10] A. Filipe, A. Schuhl and P. Galtier, *Appl. Phys. Lett.* 70 (1997) 129.
- [11] Q. Xue, T. Hashizume, J.M. Zhou, T. Sakata, T. Ohno and T. Sakurai, *Phys. Rev. Lett.* 74 (1995) 3177.
- [12] H.-P. Schönherr, R. Nötzel, W. Ma and K.H. Ploog, *J. Appl. Phys.* 89 (2001) 169.
- [13] G. Wedler, B. Wasserman, R. Nötzel and R. Koch, *Appl. Phys. Lett.* 78 (2001) 1270.
- [14] R.A. Gordon, E.D. Crozier, D.-T. Jiang, T.L. Monchesky and B. Heinrich, *Phys. Rev. B* 62 (2000) 2151.

- [15] S.M. Heald, D.L. Brewster, E.A. Stern, K.H. Kim, F.C. Brown, D.T. Jiang, E.D. Crozier and R.A. Gordon, *J. Synch. Rad.* 6 (1999) 347.
- [16] D.T. Jiang and E.D. Crozier, *Can. J. Phys.* 76 (1998) 621.
- [17] J. Stöhr, in *X-Ray Absorption Spectroscopy: Applications, Techniques of EXAFS, SEXAFS and XANES*, Eds. D.C. Koningsberger and R. Prins (Wiley, New York, 1988), Chpt. 10.
- [18] H. Oyanagi, K. Sakamoto, R. Shido, Y. Kuwahara and K. Haga, *Phys. Rev. B* 52 (1995) 5824.
- [19] P.L. Le Fevre, H. Magnan, O. Heckmann, V. Brios and D. Chandris, *Phys. Rev. B* 52 (1995) 11462.
- [20] E.D. Crozier, *Nucl. Instrum. Meth. Phys. Res. B* 133 (1997) 134.
- [21] R.A. Gordon, E.D. Crozier, J. Shoults and D.-T. Jiang, *Rev. Sci. Instrum.* 73 (2002) 2849.
- [22] J.W. Freeland, I. Coulthard, W.J. Antel Jr. and A.P.J. Stampfl, *Phys. Rev. B* 63 (2001) 193301.
- [23] M. Newville, P. Livins, Y. Yacoby, E.A. Stern and J.J. Rehr, *Phys. Rev. B* 47 (1993) 14126.
- [24] S.I. Zabinsky, J.J. Rehr, A. Ankudinov, R.C. Albers and M.J. Eller, *Phys. Rev. B* 52 (1995) 2995.
- [25] T. Ressler, *J. Phys. IV* 7 (1997) C2-269.
- [26] E.D. Crozier, A.J. Seary, M.K. McManus and D.T. Jiang, *J. Phys. IV* 7 (1997) C2-251.
- [27] W.A. Brantley, *J. Appl. Phys.* 44 (1973) 534.
- [28] J. Hornstra and W.J. Bartels, *J. Cryst. Growth* 44 (1978) 513.
- [29] B. Heinrich, M. Kowalewski and J.F. Cochran, *Can. J. Chem.* 76 (1998) 1595.

[30] S. Chikazumi and S.H. Charap, *Physics of Magnetism* (Wiley, New York, 1964) p. 173.

[31] F.W. Lee, *Rep. Prog. Phys.* 18 (1955) 184.

[32] Karl Rudolf Bauchspiess, Ph.D. thesis, Simon Fraser University, 1990. A Study of the Pressure-induced Mixed Valence Transition in SmSe and SmS by X-ray Absorption Spectroscopy.

[33] O. Moze, C. Greaves, F. Bouree-Vigneron, B. Cockayne, W.R. MacEwan, N.A. Smith and I.R. Harris, *J. Phys. Condens. Matter* 6 (1994) 10435.

[34] P. Villars and L.D. Calvert, *Pearson's Handbook of Crystallographic Data for Intermetallic Phases*, 2nd ed. (ASM International, Materials Park, OH, USA, 1991).

Figure Captions.

Figure 1. The body-centered-cubic structure is shown from an XAFS perspective with central atom **0** absorbing the X-ray and first near-neighbours, **1**, and second near-neighbours, **2**, scattering the emitted photoelectron in the case of: a) unpolarized X-rays, b) X-rays polarized with the electric field vector, **E**, along the *c*-axis, and c) X-rays polarized in the *ab*-plane with electric field vector along the $\langle 110 \rangle$ direction.

Figure 2. Comparison of XANES spectra with changing thickness for both in-plane and out-of-plane polarizations for films of thickness $\frac{1}{2}$ ML, 5 ML, 9.3 ML, 16 ML and iron foil. First derivatives are also shown to illustrate changing features just above the absorption edge (7111 eV). Curves have been normalized to edge jump and offset.

Figure 3. Overlay of XANES spectra for iron foil, 5 ML film and iron (II) oxide illustrating the absence of a dramatic edge shift for the film and differences in absorption above 7111 eV.

Figure 4. EXAFS interference functions, $\chi(k)$, with X-ray polarization a) out-of-plane along $\langle 001 \rangle$, and b) in-plane along $\langle 110 \rangle$ for iron films 0.5 to 30 monolayers thick.

Figure 5. Magnitude of the k^2 -weighted Fourier transforms of the out-of-plane (a) and in-plane (b) $\chi(k)$ for iron films 0.5 to 30 ML thick on GaAs(001)-4x6. The data were transformed over the range typically 2.4 to 14 \AA^{-1} with a 10% Gaussian window. The electron scattering process introduces a phase shift that causes peaks to appear at radial distances shorter than the actual bond lengths.

Figure 6. Fit results for first (R_1) and second (R_2) nearest neighbour distances (left) and mean-square-relative-displacements, σ^2 (right). Solid lines indicate trends for out-of-plane results while dashed lines are for in-plane fit results. For in-plane R_1 values, the dashed line represents the average excluding the 9.3 ML data which was taken with a different substrate orientation

(010) than the other thicknesses (110). Bulk iron and gallium arsenide values for first and second near neighbour distances are also given for comparison.

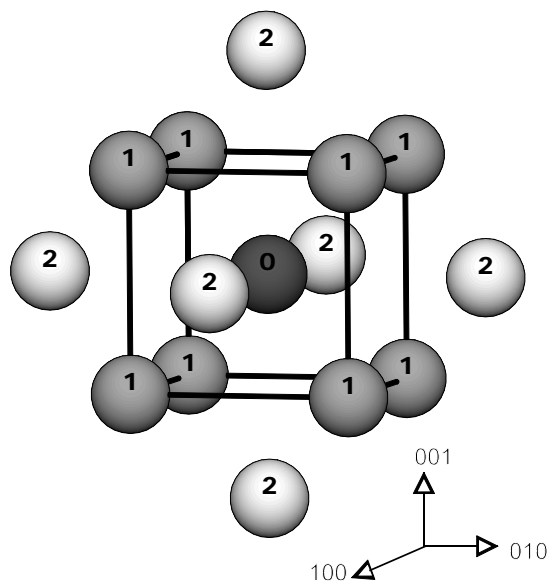


fig 1a

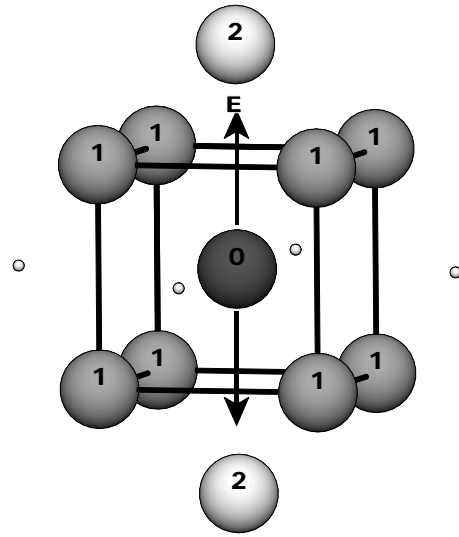


fig 1b

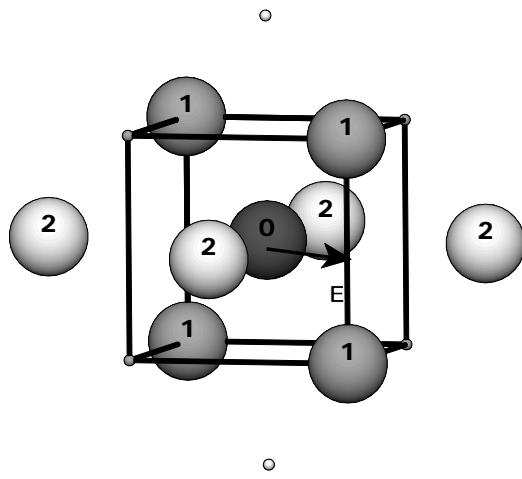


fig 1c

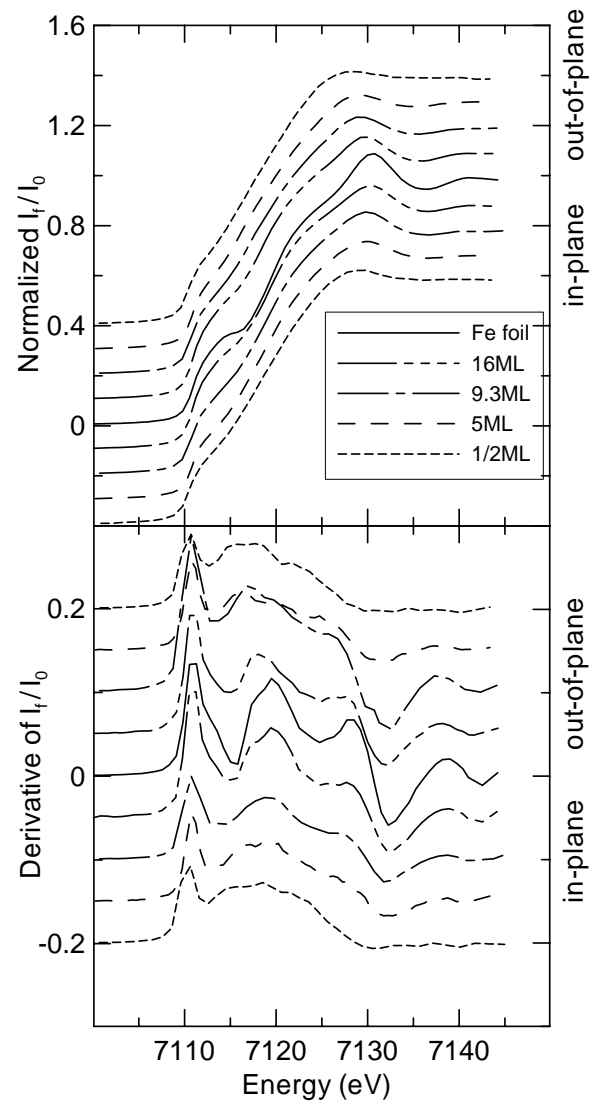


fig. 2

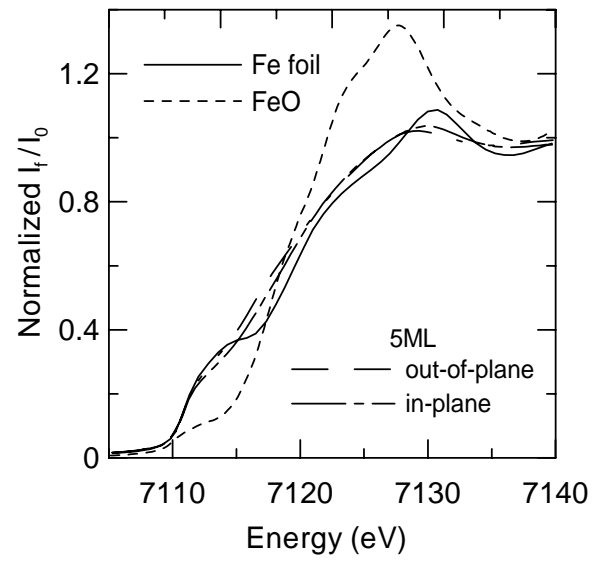


fig. 3

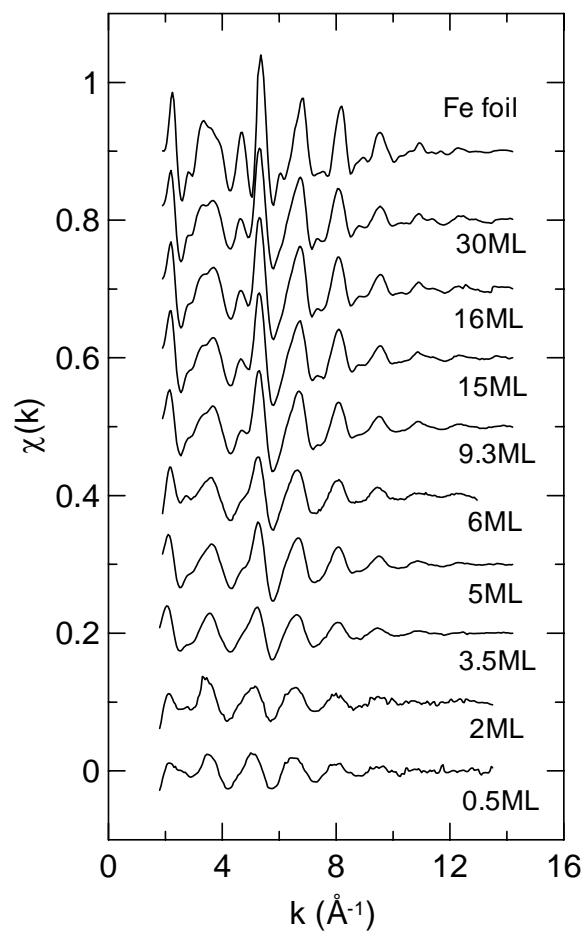


fig. 4a

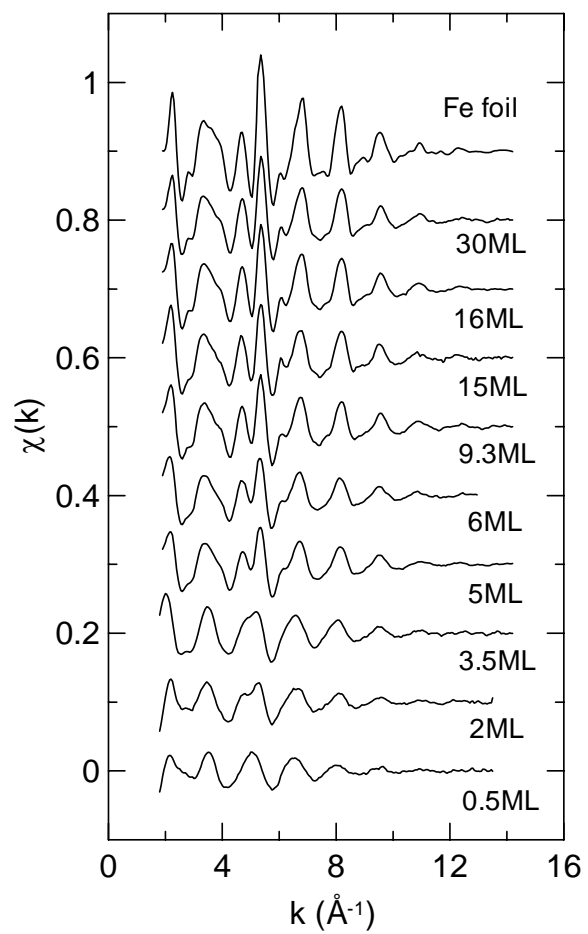


fig. 4b

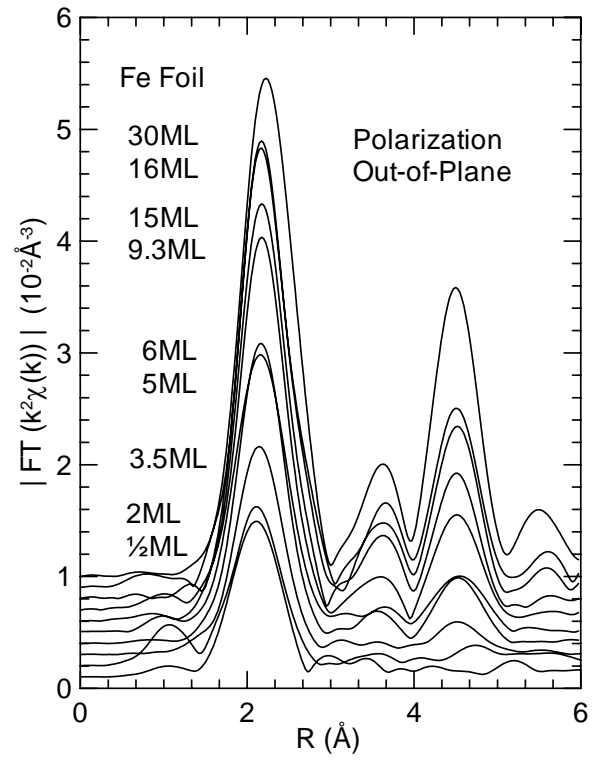


fig. 5a

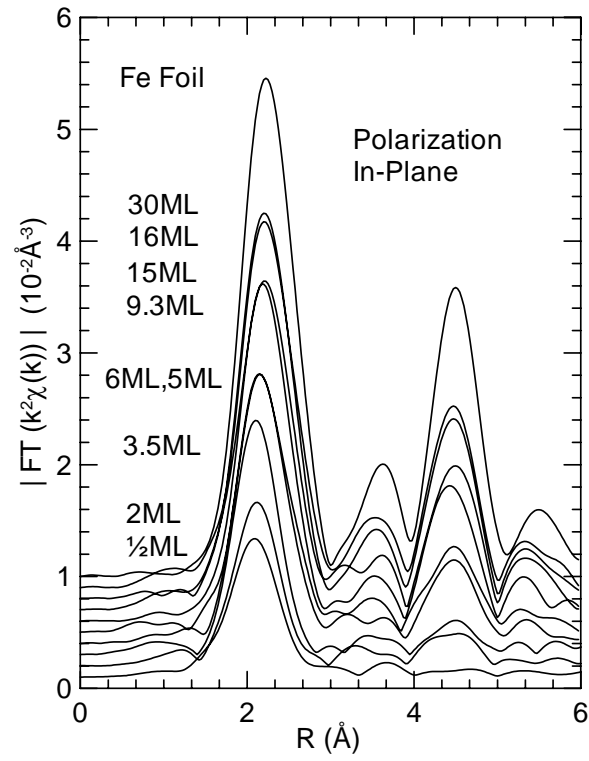


fig. 5b

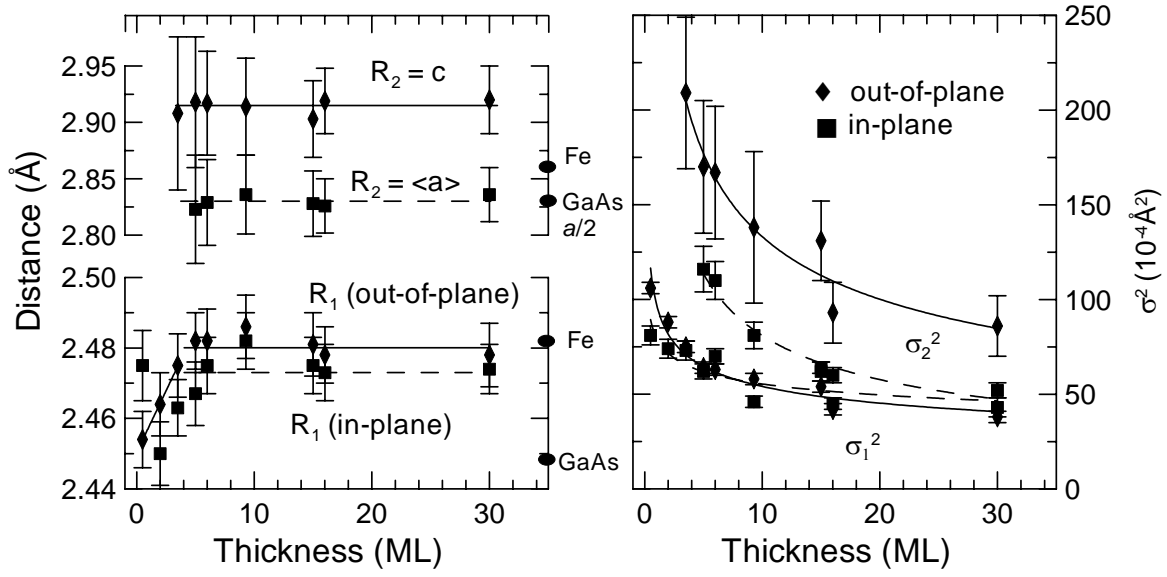


fig. 6